Annual/semiannual variation of the ionosphere

Liying Qian,[1] Alan G. Burns,[1] Stanley C. Solomon,[1] and Wenbin Wang[1]

Received 22 February 2013; revised 2 April 2013; accepted 3 April 2013; published 30 May 2013.

[1] We investigated the relationship between the systematic annual and semiannual variations in the ionosphere and thermosphere using a combination of data analysis and model simulation. A climatology of daytime peak density and height of the ionospheric F_2 layer was obtained from GPS radio occultation measurements by the Constellation Observing System for Meteorology, Ionosphere, and Climate (COSMIC) during 2007–2010. These measurements were compared to simulations by the NCAR Thermosphere-Ionosphere-Electrodynamics General Circulation Model (TIE-GCM). Model reproduction of the ionospheric annual and semiannual variations was significantly improved by imposing seasonal variation of eddy diffusion at the lower boundary, which also improves agreement with thermospheric density measurements. Since changes in turbulent mixing affect both the thermosphere and ionosphere by altering the proportion of atomic and molecular gases, these results support the proposition that composition change drives the annual/semiannual variation in both the neutral and ionized components of the coupled system. **Citation:** Qian, L., A. G. Burns, S. C. Solomon, and W. Wang (2013), Annual/semiannual variation of the ionosphere, *Geophys. Res. Lett.*, *40*, 1928–1933, doi:10.1002/grl.50448.

1. Introduction

[2] The *F* region ionosphere is influenced by many aspects of the neutral thermosphere in which it is embedded, including its temperature, its wind field, and its composition, particularly the relative proportion of atomic and molecular components. Both the ionosphere and thermosphere have well-known diurnal cycles and vary in response to solar ultraviolet irradiance and geomagnetic activity. Equally important to their climatology, but less frequently discussed, are the systematic semiannual and annual variations seen in thermosphere parameters such as composition and mass density [e.g., *Qian et al*., 2009] and in ionosphere parameters such as the peak electron density of the F_2 layer (N_mF_2) [e.g., *Rishbeth*, 1998; *Mendillo et al*., 2005]. However, the relationship between the annual/semiannual variations in the thermosphere and the apparently similar variations in the ionosphere has not been clearly established, and, if there is a causal relationship, the mechanism has not been explicated.

[3] The annual variation of N_mF_2 at the solstices is referred to as annual asymmetry. Global mean N_mF_2 is typically about 30% greater in December–January than that in June–July, which cannot be fully explained by the 7% ionization rate change caused by the difference in Sun-Earth distance between the two solstice seasons. *Mendillo et al*. [2005] analyzed ground-based total electron content measurements from the global GPS network and neutral composition data from the Global Ultraviolet Imager (GUVI) on the Thermosphere-Ionosphere-Mesosphere Energetics and Dynamics (TIMED) satellite, concluding that changes in neutral composition could be partly responsible for the asymmetry. *Rishbeth and Muller-Wodarg* [2006] investigated the annual asymmetry using simulations by the Coupled Thermosphere-Ionosphere-Plasmasphere (CTIP) model [*Fuller-Rowell et al*., 1996]. They found it unlikely that various possible causes, including asymmetry of the geomagnetic field, auroral zone, large-scale dynamics, and upward propagating tides, had sufficiently large effect. They concluded that the dynamical influence of the lower atmosphere, which is not included in the CTIP model, is a possible cause of the annual asymmetry. This idea was further expanded by *Rishbeth* [2006]. *Zeng et al*. [2008] performed modeling investigations of the annual asymmetry, comparing data from Constellation Observing System for Meteorology, Ionosphere, and Climate (COSMIC) during 2006 to TIE-GCM simulations and found that the displacement of the geomagnetic field axis from the geographic axis and the change in Sun-Earth distance were primary causes.

[4] The semiannual variation of N_mF_2, where the equinoxes are systematically larger than the solstices, is as prominent as the annual asymmetry, but its mechanism is also unknown. *Rishbeth* [1998] speculated on the possible role of semiannual oscillations in the lower or middle atmosphere on the semiannual variation of N_mF_2 but did not elaborate on it. The strong semiannual variation of thermospheric neutral density and atomic/molecular composition is an obvious candidate mechanism, but although the general circulation of the thermosphere [*Fuller-Rowell*, 1998] partly causes this effect, it is insufficient in magnitude to explain it. *Qian et al*. [2009] simulated annual/semiannual thermospheric composition and density climatology and obtained agreement with measurements by applying a seasonal term to the parameterization of eddy diffusion at the lower boundary of the TIE-GCM. They proposed that lower atmosphere dynamics were the underlying cause. Refer to that paper for further discussion of seasonal variations in the thermosphere.

[5] In this paper, we examine both the annual and semiannual variations of the F_2 peak, based on a daytime global climatology derived from 4 years of COSMIC data (2007–2010). Through model simulations, we demonstrate the importance of neutral composition to the annual and semiannual variation of ionospheric structure and that neutral composition can respond strongly to seasonal changes in turbulent mixing near the mesopause.

[1]High Altitude Observatory, National Center for Atmospheric Research, Boulder, Colorado, USA.

Corresponding author: L. Qian, High Altitude Observatory, National Center for Atmospheric Research, Boulder, Colorado, USA. (lqian@ucar.edu)

0094-8276/13/10.1002/grl.50448

2. Measurements by the COSMIC Satellites

[6] The COSMIC satellites have made GPS radio occultation observations of ionosphere electron density profiles since 2006. Although there are some issues involved with obtaining full electron density profiles in the presence of horizontal gradients [e.g., *Yue et al*., 2010], the peak density N_mF_2 and height h_mF_2 of the F_2 layer can be obtained with good accuracy and precision, and these measurements have been validated through comparison to ground-based observations [e.g., *Lei et al*., 2007]. *Burns et al*. [2012] constructed a 4 year daytime global climatology of ionospheric N_mF_2 and h_mF_2, using this global ionospheric data set, from 2007 to 2010. They found that low-latitude N_mF_2 was dominated by annual/semiannual variations, where N_mF_2 had maxima near the equinoxes, a primary minimum near the June solstice, and a secondary minimum near the December solstice, and that these annual/semiannual variations extended to midlatitudes. The h_mF_2 also showed a pronounced annual variation, with the highest values of h_mF_2 occurring at low latitudes and on the summer side of the magnetic equator and minimum values at middle latitudes in winter.

3. Model Description

[7] The model employed in this study is the National Center for Atmospheric Research (NCAR) Thermosphere-Ionosphere-Electrodynamics general circulation model (TIE-GCM). The TIE-GCM is a community model developed at the NCAR High Altitude Observatory, publicly available at www.hao.ucar.edu. It is a first-principles upper atmosphere general circulation model that solves the Eulerian continuity, momentum, and energy equations for the coupled thermosphere/ionosphere system, covering the altitude range from approximately 97 km to 600 km [*Roble et al*., 1988; *Richmond et al*. 1992; *Qian et al*., 2012]. It has a horizontal resolution of $5^\circ \times 5^\circ$ and a vertical resolution of one half pressure scale height. The main external drivers of the TIE-GCM are solar irradiance in the extreme-ultraviolet and far-ultraviolet spectral regions, geomagnetic energy including auroral particle precipitation and ionospheric convection, and perturbation at the lower boundary of the model by tides and waves. In this study, the Extreme Ultra-Violet flux model for Aeronomic Calculation (EUVAC) solar proxy model [*Richards et al*., 1994] was used as solar input [*Solomon and Qian*, 2005], but the MgII core-to-wing ratio [*Viereck et al*., 2004] scaled to the range of the $F_{10.7}$ index [*Solomon et al*., 2011] was used as the solar activity index instead of the regular $F_{10.7}$ index. This is to accommodate difficulties with the $F_{10.7}$ index during the 2008–2009 solar minimum [*Solomon et al*., 2010], which is an important period of the COSMIC data used in this paper. Ionospheric convection is specified by the empirical model of *Heelis et al*. [1982], and migrating semidiurnal and diurnal tides are applied at the lower boundary using the Global Scale Wave Model (GSWM) [*Hagan and Forbes*, 2002; 2003], which provides climatological monthly mean hourly tides given at the middle of each month. The model reads GSWM tides and linearly interpolates these to other dates. The effect of turbulent mixing, mainly due to gravity wave breaking in the mesosphere-lower-thermosphere (MLT) region, is included by specifying a latitude-dependent eddy diffusion coefficient at the lower boundary.

4. Results

4.1. Initial Model-Data Comparisons

[8] The TIE-GCM was run from 2007 to 2010. The simulated results were sampled in the same way that COSMIC data were processed by *Burns et al*. [2012]: a 30-day running median was applied to the daily medians of each geomagnetic latitude bin (10°) to remove the short-term variability. Figure 1 compares the daytime climatology of N_mF_2 and h_mF_2 observed by COSMIC and simulated by the TIE-GCM. The model simulations have a similar solar cycle variability. However, there are large differences between the model and the data in terms of the annual/semiannual variations. COSMIC N_mF_2 shows distinct and consistent annual and semiannual variations at low latitudes ($\pm 30^\circ$ magnetic latitudes), with maxima near the equinoxes, a primary minimum near the June solstice, and a secondary minimum near the December solstice. The model-simulated N_mF_2 lacks this annual/semiannual variation, except for a consistent peak at the March equinox. In both hemispheres, COSMIC N_mF_2 shows an annual/semiannual variation at midlatitudes that transitions to an annual variation at the high latitudes, with higher values of N_mF_2 in summer than in winter. However, the simulated N_mF_2 shows an annual variation at midlatitudes to high latitudes with higher values of N_mF_2 in winter rather than in summer.

[9] The highest values of h_mF_2 in the COSMIC data occur at low latitudes and on the summer side of the magnetic equator throughout the 4 year period (Figure 1c). The COSMIC h_mF_2 exhibits annual variations, with highs in summer and lows in winter, at all latitudes except the northern polar latitudes. This annual variation in the COSMIC h_mF_2 is consistent with solar zenith angle effects and, therefore, can be easily explained by the winter-summer variations of solar heating. In addition, prevailing neutral winds, which blow from the summer hemisphere to the winter hemisphere, can increase h_mF_2 in the summer hemisphere and decrease it in the winter hemisphere, also contributing to the annual variation seen in the COSMIC h_mF_2 [*Burns et al*., 2012].

[10] At low latitudes ($\pm 30^\circ$ magnetic latitudes), the model-simulated h_mF_2 shows a similar annual variation, although the simulated h_mF_2 is overall higher than the data. At midlatitudes and high latitudes, however, the simulated h_mF_2 shows an annual variation in both hemispheres with highs in winter and lows in summer that is opposite to the annual variation seen in the data.

[11] What could be the cause of these discrepancies? It is important to note that the correct geomagnetic field configuration and the Sun-Earth distance, the two main factors that contributed to the annual asymmetry of N_mF_2 in the model simulations of *Zeng et al*. [2008], are already included in these simulations. In order to answer this question, we need to investigate the external forcing of the model, since the thermosphere/ionosphere system is mainly an externally driven system. Here, we focus on turbulent mixing processes at the lower boundary of the model, as parameterized by the eddy diffusion coefficient.

4.2. Eddy Diffusion and Its Impact on Neutral Composition and Density

[12] Little is known about the magnitude and variability of turbulent mixing processes in the mesopause region due to limited observations of the turbulence produced as waves

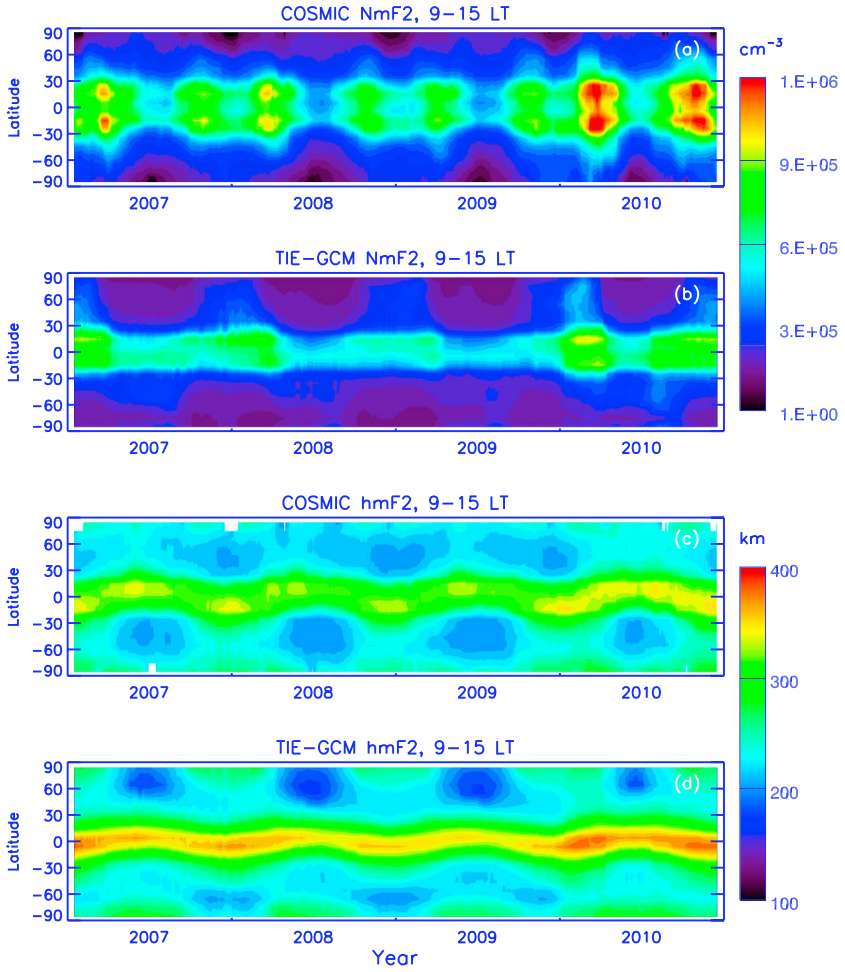

Figure 1. Model-data comparisons of N_mF_2 and h_mF_2 climatology from 2007 to 2010 in magnetic latitude bins. (a) N_mF_2 observed by COSMIC. Each magnetic latitude bin was calculated using the median of data from all longitudes for local times between 09:00 and 15:00. The data were then further processed by taking a 30 day running median for each bin, in order to remove short-term variability; (b) TIE-GCM simulated N_mF_2, processed the same way as the data; (c) h_mF_2 observed by COSMIC. h_mF_2 was processed the same way as that for N_mF_2; (d) TIE-GCM simulated h_mF_2, processed the same way as the data.

propagate upwards. As a result, the standard version of the TIE-GCM has a simplified parameterization of this process. An eddy diffusion coefficient is applied at the model lower boundary that is constant (125 m^2/s) with respect to day of year. Latitudinal variation is estimated by applying an inverse sinusoid function, with a minimum at the equator:

$$K_E(\lambda,0) = K_E[0.25 + 0.5 \times (1 + \sin(4.5|\lambda| - \pi/2))],$$
$$\text{where } |\lambda| < \frac{\pi}{4.5}$$
$$K_E(\lambda,0) = K_E \times 1.25, \quad \text{where} |\lambda| \geq \frac{\pi}{4.5}$$

where $K_E(\lambda,0)$ is the eddy diffusion coefficient at the lower boundary at latitude λ (in radians), and K_E is the nominal eddy diffusion coefficient value of 125 $m^2 s^{-1}$. Above the lower boundary, the eddy diffusion coefficient decreases exponentially with increasing altitude:

$$K_E(\lambda,z) = K_E(\lambda,0) \times e^{(-7-z)}$$

where z is the TIE-GCM pressure coordinate, $z = \ln(P_0/P)$, and P_0 is the reference pressure of 5×10^{-7} hPa. The lower boundary of the TIE-GCM is at $z = -7$, which is at about 97 km. At the lower boundary, the mass mixing ratio of the major species O_2 and N_2 are specified as 0.22 and 0.78, respectively. The vertical gradient of atomic oxygen (O) number density is specified as zero at the lower boundary. Therefore, O is effectively lost from the lower boundary of the model. Increasing eddy diffusion accelerates downward transport and removal of O, thereby decreasing O in the model.

[13] Various measurements of gravity wave breaking have indicated that there are strong seasonal variations due to both changes in the gravity wave sources and variations in gravity wave propagation through the middle atmosphere [e.g., *Garcia and Solomon*, 1985; *Akmaev*, 2001]. Limited observations of MLT eddy diffusion have also suggested that eddy diffusion has a seasonal variation with lows during the equinoxes and highs during the solstices [e.g., *Fukao et al.*, 1994; *Khattatov et al.*, 1997].

[14] Previous model-data comparisons of thermospheric neutral density [*Qian et al.*, 2009] showed that neutral density modeled by the TIE-GCM lacked an annual/semiannual variation that is clearly and persistently seen in measurements [e.g., *Bowman*, 2004; *Emmert*, 2009;

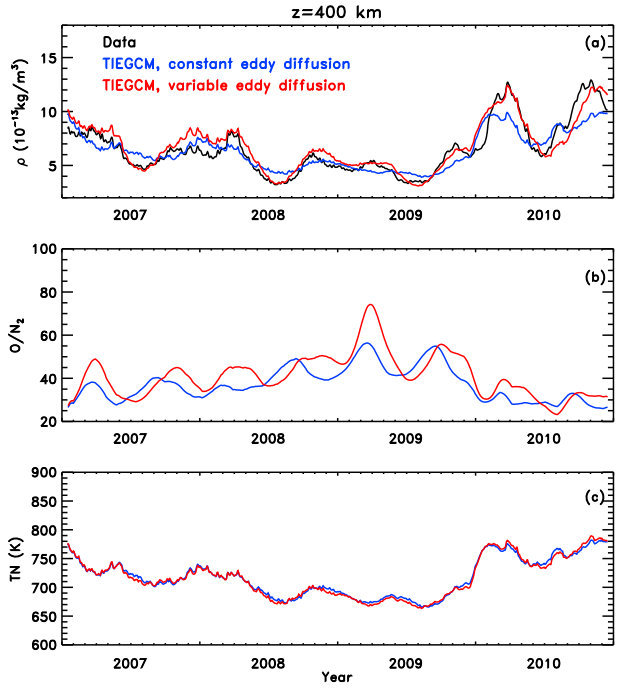

Figure 2. Thermosphere parameters at 400 km. (a) Model-data comparisons of global mean neutral density at 400 km. Black: neutral density derived from drag data of more than 5000 space objects [*Emmert*, 2009]; red: TIE-GCM simulations when the variable eddy diffusion was imposed at the model lower boundary; blue: TIE-GCM simulations when the default constant eddy diffusion was imposed at the model lower boundary. (b) Global mean O/N_2; same color scheme. (c) Global mean neutral temperature; same color scheme.

Qian and Solomon, 2011]. Figure 2a shows model-data comparisons of global mean neutral density at 400 km from 2007 to 2010, derived from drag data of more than 5000 space objects [*Emmert*, 2009] (black), simulated by the TIE-GCM using the default eddy diffusion parameterization (blue) and simulated by the TIE-GCM using the variable eddy diffusion (red). The drag data shows a consistent annual/semiannual variation with highs near the equinoxes, a primary low near the June solstice, and a secondary low near the December solstice for every year. The simulated neutral density using the default constant eddy diffusion failed to replicate the annual/semiannual variation (Figure 2a, blue). From these comparisons, an ad hoc function was derived for the seasonal variation of eddy diffusion [cf. *Qian et al.*, 2009, Figure 6]. The variable eddy diffusion coefficient maximizes near solstices, with the primary maximum near the June solstice (~250 m^2/s), and minimizes near equinoxes (~40 m^2/s). It has an annual average value that is close to the default constant. In this paper, constant (variable) eddy diffusion refers to constant (variable) with respect to day of year.

[15] When the variable eddy diffusion was imposed at the model lower boundary, the simulated neutral density shows an annual/semiannual variation that is largely consistent with the data (Figure 2a, red). Neutral density is determined by neutral temperature and composition. Figure 2b compares the simulated global mean neutral composition (O/N_2) at 400 km, using the default constant eddy diffusion coefficient (blue) versus using the variable eddy diffusion (red), whereas Figure 2c is the corresponding comparison for global mean neutral temperature at 400 km. Eddy diffusion impacts neutral density mainly by changing thermospheric composition. Eddy diffusion transports atomic oxygen downward, against the mixing ratio gradient, from the lower thermosphere into the mesopause region, where it is destroyed by three-body recombination, and thus reduces the O/N_2 in the thermosphere. This effect is evident by examining O/N_2 shortly after the June solstice of each year in Figure 2b. Large eddy diffusion during these time periods when the variable eddy diffusion was imposed (red) reduces the O/N_2 and thus reduces neutral density, causing the simulated neutral density to be more consistent with the data (Figure 2a). The effect of eddy diffusion on neutral temperature is relatively small (Figure 2c). Figure 2 demonstrates that eddy diffusion changes composition in the thermosphere and thus influences neutral density. The imposition of the variable eddy diffusion causes the TIE-GCM O/N_2 to exhibit an annual/semiannual pattern that is more consistent with the O/N_2 observed by the GUVI instrument aboard the TIMED satellite, as well as an improved representation of neutral density [cf. *Qian et al.*, 2009, Figures 9 and 10].

4.3. Eddy Diffusion and Its Effect on the F_2 Peak

[16] We conducted model-data comparisons of F region ionospheric parameters using variable eddy diffusion at the TIE-GCM lower boundary. These simulations reproduced the main observed features of N_mF_2, including the equinoctial peaks and the annual anomaly, at low latitudes (±30° magnetic latitudes) as shown in Figures 3a and 3b. Diagnostic analysis indicated that this improvement was mainly caused by composition change due to the variable eddy diffusion. An increase in the ratio of atomic-to-molecular constituents results in an increase in daytime ionospheric density. This is a consequence of the balance of solar ionization production rates (approximately proportional to the atomic oxygen density in the F region) and chemical recombination loss rates (approximately proportional to the molecular density, primarily N_2 and O_2).

[17] In the Southern Hemisphere midlatitudes (−30° to −60°), the model-simulated N_mF_2 shows an annual/semiannual variation that is present in the data but is absent in the baseline runs shown in Figure 1b. Similarly, the model-simulated h_mF_2 shows an annual variation with lows in winter and highs in summer at these latitudes (Figure 3d), which is consistent with the data, but with less amplitude. This improves upon the simulated h_mF_2 that was calculated using constant eddy diffusion, which exhibited the opposite behavior at these latitudes (Figure 1d). In the Northern Hemisphere midlatitudes, however, the simulated N_mF_2 and h_mF_2 still shows unrealistically low summer values in both parameters, and high winter values, which are not supported by the observations.

[18] In summary, imposing variable eddy diffusion greatly improved the annual/semiannual variation of N_mF_2 at low latitudes (±30° magnetic latitudes), and it also improved N_mF_2 and h_mF_2 at midlatitudes in the Southern Hemisphere. However, imposing the variable eddy diffusion did not solve the summer-to-winter variation shown in the

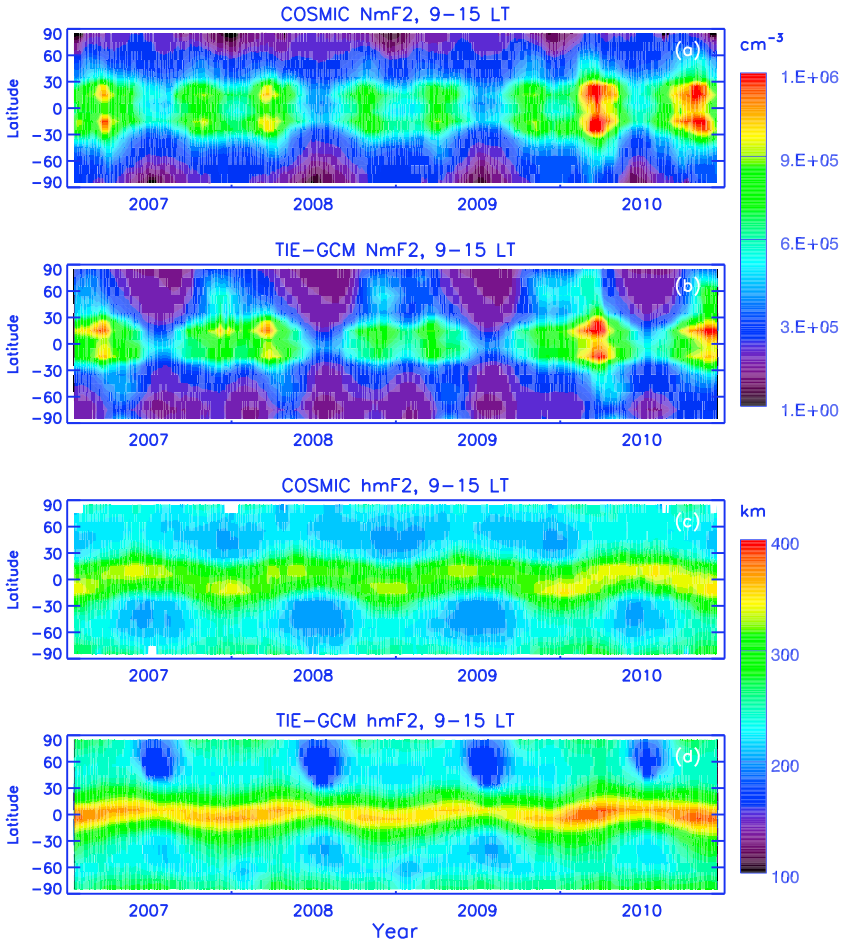

Figure 3. The same as Figure 1, except that Figure 1 shows the model-data comparisons when the default constant eddy diffusion was imposed at the model lower boundary, but this figure shows the model-data comparisons when the variable eddy diffusion was imposed at the model lower boundary.

simulated h_mF_2 and N_mF_2 in the northern midlatitudes and high latitudes and also has some remaining discrepancies at the southern high latitudes.

5. Discussion and Conclusions

[19] The causes of the annual and semiannual variations in N_mF_2 are not fully understood. However, the model-data comparisons suggest that variable eddy diffusion may play an important role in the observed variation of N_mF_2 at low latitudes. The effect of eddy diffusion on the low-latitude N_mF_2 correspond to the effects of eddy diffusion on thermosphere composition and neutral density, since large values of O/N_2 correspond to large values of N_mF_2. The central conclusion of this study is that the same adjustment to the lower boundary of the TIE-GCM that improves comparison with observed neutral density and composition climatology simultaneously improves comparison with observed ionospheric F region climatology.

[20] The eddy diffusion coefficient applied to the model lower boundary is in effect a surrogate for all microscale or mesoscale mixing processes that are not captured by the model, regardless of cause. The actual mechanisms by which the lower and middle atmospheres produce variability in vertical transport at and above the mesopause are complex and remain uncertain, but it is clear that there are systematic seasonal variations. There must be interannual variations as well, but the general features of the annual pattern are clear and repeatable. Understanding the dynamical causes of this phenomenon is a central challenge for upper atmosphere modeling.

[21] Imposing seasonally variable eddy diffusion on a global basis did not solve all the discrepancies in the model. The two hemispheres have different seasonal patterns, and there must be a latitude dependence to the variation. Since the asymmetry between atmospheric dynamics in the two hemispheres is an underlying cause of the annual term of global changes in composition, and hence in neutral and electron density, a more sophisticated treatment of the latitudinal variation of eddy diffusion coefficient is clearly indicated.

[22] The composition changes induced by this method also did not solve the issue with winter-to-summer variation in the model. Some other processes are likely responsible for this discrepancy. At the F_2 peak, several transport processes are important in determining its magnitude and altitude, including ambipolar diffusion, neutral winds, and *ExB* drift. In addition, the transport of ions in and out of the plasmasphere has a significant effect, which is approximated in this model formulation by an assumed flux applied as an upper boundary condition. Future work will investigate the processes that are responsible for this problem.

[23] **Acknowledgments.** This research was supported by NASA grants NNX08AQ31G NNX10AF21G, NNX10AQ59G, and NNX09AJ60G to the National Center for Atmospheric Research and by the Center for Integrated Space Weather Modeling (CISM), which is funded by the National Science Foundation under agreement ATM-0120950. NCAR is sponsored by the National Science Foundation.

[24] The Editor thanks two anonymous reviewers for their assistance in evaluating this paper.

References

Akmaev, R. A. (2001), Simulation of large-scale dynamics in the mesosphere and lower thermosphere with the Doppler-spread parameterization of gravity waves 2. Eddy mixing and the diurnal tide, *J. Geophys. Res.*, *106*, 1205–1213.

Bowman, B. R. (2004), The semiannual thermosphere density variation from 1970 to 2002 between 200-1100 km, AAS 2004–174, AAS/AIAA Spaceflight Mechanics Meeting, Maui, Hi, February. Davies, K. (1990), Ionospheric Radio, Peter Peregrinus, London.

Burns, A. G., S. C. Solomon, W. Wang, L. Qian, Y. Zhang, and L. J. Paxton (2012), Daytime climatology of ionospheric N_mF_2 and hmF2 from COSMIC data, *J. Geophys. Res.*, *117*, A09315, doi:10.1029/2012JA017529.

Emmert, J. T. (2009), A long-term data set of globally averaged thermospheric total mass density, *J. Geophys. Res.*, *114*, A06315, doi:10.1029/2009JA014102.

Fukao, S., M. D. Yamanaka, N. Ao, W. K. Hocking, T. Sato, M. Yamamoto, T. Nakamura, T. Tsuda, and S. Kato (1994), Seasonal variability of vertical eddy diffusivity in the middle atmosphere 1. Three-year observations by the middle and upper atmosphere radar, *J. Geophys. Res.*, *99*, 18973–18987.

Fuller-Rowell, T. J. (1998), The "thermospheric spoon": A mechanism for the semiannual density variation, *J. Geophys. Res.*, *103*, 3951–3956.

Fuller-Rowell, T. J., D. Rees, S. Quegan, R. J. Moffett, M. V. Codrescu, and G. H. Millward (1996), *A Coupled Thermosphere-Ionosphere Model (CTIM), STEP Handbook of Ionospheric Models*, edited by R.W. Schunk, 217–238 pp. Utah State University, Logan, Utah.

Garcia, R. R., and S. Solomon (1985), The effect of breaking gravity waves on the dynamics and chemical composition of the mesosphere and lower thermosphere, *J. Geophys. Res.*, *90*, 3850–3868.

Hagan, M. E., and J. M. Forbes (2002), Migrating and nonmigrating diurnal tides in the middle and upper atmosphere excited by tropospheric latent heat release, *J. Geophys. Res.*, *107*(D24), 4754, doi:10.1029/2001JD001236.

Hagan, M. E., and J. M. Forbes (2003), Migrating and nonmigrating semidiurnal tides in the upper atmosphere excited by tropospheric latent heat release, *J. Geophys. Res.*, *108*(A2), 1062, doi:10.1029/2002JA009466.

Heelis, R. A., J. K. Lowell, and R. W. Spiro (1982), A model of the high-latitude ionospheric convection pattern, *J. Geophys. Res.*, *87*, 6339–6345.

Khattatov, B. V., M. A. Geller, and V. A. Yubin (1997), Diurnal migrating tides as seen by the high-resolution Doppler imager/UARS 2. Monthly mean global zonal and vertical velocities, pressure, temperature, and inferred dissipation, *J. Geophys. Res.*, *102*, 4423-4435.

Lei, J., et al. (2007), Comparison of COSMIC ionospheric measurements with ground based observations and model predictions: Preliminary results, *J. Geophys. Res.*, *112*, A07308, doi:10.1029/2006JA012240.

Mendillo, M., C. Huang, X. Pi, H. Rishbeth, and R. Meier (2005), The global ionospheric asymmetry in total electron content, *J. Atmos. Sol. Terr. Phys.*, *67*, 1377–1387.

Qian, L., and S. C. Solomon (2011), Thermospheric density: An overview of temporal and spatial variations, *Space Sci. Rev.* doi:10.1007/s11214-011-9810-Z.

Qian, L., S. C. Solomon, and T. J. Kane (2009), Seasonal variation of thermospheric density and composition, *J. Geophys. Res.*, *114*, A01312, doi:10.1029/2008JA013643.

Qian, L., A. G. Burns, B. A. Emery, B. Foster, G. Lu, A. Maute, A. D. Richmond, R. G. Roble, S. C. Solomon, and W. Wang (2012), The NCAR TIE-GCM: A community model of the coupled thermosphere/ionosphere system, *Am. Geophys. Monogr.*, doi:10.1029/2012GM001297.

Richards, P. G., J. A. Fennelly, and D. G. Torr (1994), EUVAC: A solar EUV flux model for aeronomic calculations, *J. Geophys. Res.*, *99*, 8981–8992.

Richmond, A. D., E. C. Ridley, and R. G. Roble (1992), A thermosphere/ionosphere general circulation model with coupled electrodynamics, *Geophys. Res. Lett.*, *19*, 601.

Rishbeth, H. (1998), How the thermospheric circulation affects the ionospheric F_2-layer, *J. Atmos. Sol. Terr. Phys.*, *60*, 1385–1402.

Rishbeth, H. (2006), *F*-region links with the lower atmosphere?, *J. Atmos. Solar-Terr. Phys.*, *68*, 469.

Rishbeth, H., and I. C. F. Muller-Wodarg (2006), Why is there more ionosphere in January than in July? The annual asymmetry in the F_2-layer, *Ann. Geophys.*, *24*, 3293.

Roble, R. G., E. C. Ridley, A. D. Richmond, and R. E. Dickinson (1988), A coupled thermosphere/ionosphere general circulation model, *Geophys. Res. Lett.*, *15*, 1325.

Solomon, S. C., and L. Qian (2005), Solar extreme-ultraviolet irradiance for general circulation models, *J. Geophys. Res.*, *110*, A10306, doi:10.1029/2005JA011160.

Solomon, S. C., T. N. Woods, L. V. Didkovsky, J. T. Emmert, and L. Qian (2010), Anomalously low solar extreme-ultraviolet irradiance and thermospheric density during solar minimum, *Geophys. Res. Lett.*, *37*, L16103, doi:10.1029/2010GL044468.

Solomon, S. C., L. Qian, L. V. Didkovsky, R. A. Viereck, and T. N. Woods (2011), Causes of low thermospheric density during the 2007–2009 solar minimum, *J. Geophys. Res.*, *116*, A00H07, doi:10.1029/2011JA016508.

Viereck, R. A., L. E. Floyd, P. C. Crane, T. N. Woods, B. G. Knapp, G. Rottman, M. Weber, L. C. Puga, and M. T. DeLand (2004), A composite Mg II index spanning from 1978 to 2003, *Space Weather*, *2*, S10005, doi:10.1029/2004SW000084.

Yue, X., W. S. Schreiner, J. Lei, S. V. Sokolovskiy, C. Rocken, D. C. Hunt, and Y.-H. Kuo (2010), Error analysis of Abel retrieved electron density profiles from radio occultation measurements, *Ann. Geophys.*, *28*, 217–222, doi:10.5194/angeo-28-217-2010.

Zeng, Z., A. Burns, W. Wang, J. Lei, S. Solomon, S. Syndergaard, L. Qian, and Y.-H. Kuo (2008), Ionospheric annual asymmetry observed by the COSMIC radio occultation measurements and simulated by the TIEGCM, *J. Geophys. Res.*, *113*, A07305, doi:10.1029/2007JA012897.